Motion of Charge Carriers in Normal He^4

R. M. Ostermeier and K. W. Schwarz
Department of Physics and The James Franck Institute, The University of Chicago, Chicago, Illinois 60637

(Received 29 March 1971; revised manuscript received 21 October 1971)

Values for the mobilities of positive and negative charge carriers in normal He^4 at the vapor pressure are presented. The interpretation of these measurements in terms of the usual microscopic models for the charge carriers is shown to require the correct hydrodynamic treatment of a modified Stokes-flow problem. Good agreement with experiment is found for both μ_+ and μ_- below 4.2 °K, and new information is obtained about several features of the carrier structures. The behavior of μ_+ and μ_- above 4.2 °K suggests the possibility that the viscosity of normal helium has a peculiar temperature dependence in this range. Sudden drops in μ_+ and μ_- are observed near the critical temperature, and it is argued that this kind of effect may be due to critical-point fluctuations, rather than to changes in carrier structure as has been claimed by other authors.

I. INTRODUCTION

The study of excess charges in superfluid helium has in recent years become one of the more useful means of exploring superfluid properties on a microscopic scale. Particular interest has centered on three problems: the nature of the charge carriers, their interaction with the elementary excitations comprising the normal-fluid component, and the quantum-hydrodynamic behavior of the superfluid surrounding the carriers. Of these the first is the most basic since, in addition to being of interest in itself, a thorough understanding of the charge-carrier structure is a necessary prerequisite for the intelligent interpretation of experiments in the other areas, where the carriers are used as moving probes.

Theoretical models for the structure of both the negative and the positive charge carriers are in reasonable agreement with a variety of experiments. The electron-bubble model[1] for the negative carrier has been particularly successful and, except for some details, is well established. The electrostriction model proposed by Atkins[2] for the positive carrier requires more detailed verification, as only the effective mass and some rough measures of size have been deduced from experiment.[3-5] One reason, therefore, for taking a careful look at the motion of the carriers in *normal* helium is that such an experiment offers a chance to learn more about their structure.

A second point arises from the findings of Cantelli, *et al.*[6] that charge carriers in He^3 exhibit peculiar behavior near the critical point. Such effects are potentially very interesting, since they indicate that the charge carriers may serve as useful probes for studying critical-point phenomena. The other purpose of this work was, therefore, to look for similar critical-point effects in He^4, and to attempt to understand them.

Our experiment was of the usual straightforward type—an electric field $\mathcal{E}$ is applied to the charge carriers and their equilibrium drift velocity v_D is measured. This determines the mean drag force exerted by the fluid on a carrier with mean velocity v_D, the results in the low-velocity limit being conventionally expressed in terms of the mobility

$$\mu \equiv v_D/\mathcal{E} = ev_D/(\text{drag force}) \to \text{const.}$$

The accepted models for both kinds of carrier are based on treating the fluid as a continuum, so that in the normal regime it seems at least a reasonable first approximation to approach the calculation of the drag force as a problem in classical hydrodynamics. Provided this problem can be solved, the theoretical carrier structures may then be checked against experiment in a rather straightforward way.

II. EXPERIMENT AND RESULTS

The mobility of positive and negative charge carriers in liquid He^4 was measured along the vapor-pressure curve from $T_\lambda = 2.17$ °K to $T_C = 5.18$ °K. The measurements were carried out by determining the time of flight of a pulse of the carriers under the action of a uniform electric field. This experimental method has been described previously,[7] and will be discussed in detail in a forthcoming paper.

Some special precautions were taken to ensure a reasonably well-defined temperature in the drift space. The experimental cell was mounted horizontally in a copper can with walls $\frac{1}{4}$ in. thick. This can was immersed in the helium bath, and the sample helium was condensed into the can after passing through liquid-nitrogen-cooled charcoal traps. The temperature in the sample chamber was kept constant by bringing the helium bath to the desired temperature, and then controlling it by means of an ac bridge. The temperature-sensing element for the bridge was mounted inside the sample chamber at the level of the drift space, while the controlling

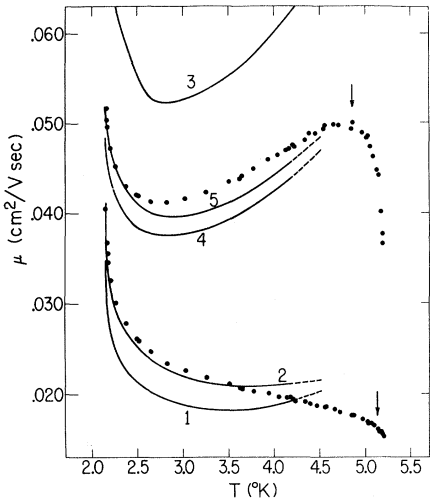

FIG. 1. Mobility at the vapor pressure in normal liquid helium. The lower line of points are the values measured for negative charge carriers, the upper line of points shows the results for positive charge carriers. Curves 1–5 are discussed in the text.

heater consisted of a wire wound uniformly around the outside of the can, in contact with the bath.

The temperature of the He^4 in the drift space was measured in two different ways. The primary method was to measure the vapor pressure of the liquid in the can. As a check on this, a carbon resistor was mounted inside the can at the level of the drift space and calibrated against the vapor pressure for temperatures below the λ point, where thermal gradients are insignificant. The resulting curve of resistance vs temperature was extrapolated into the normal regime and used to determine the temperature at the level of the drift space. These two methods agreed to within 0.02 °K everywhere, and we take this as our uncertainty in T. Since the mobilities vary relatively slowly with temperature in normal helium, an uncertainty of 0.02 °K can be tolerated.

Our measured values of the mobilities are shown in Fig. 1, the estimated absolute errors being less than 2%. Previous determinations of lesser accuracy have been reported for $T \leq 4.2$ °K by various authors.[8–10] These generally fall within about 20% of our data.

III. DISCUSSION

A. Hydrodynamic Problem

The negative charge carrier consists of an electron localized in a bubble[1] from which the He^4 atoms are excluded. The equilibrium radius of the bubble can be calculated by minimizing its total energy,[11] and is of course a function of temperature, varying from about 16 Å at T_λ to about 20 Å at T_C. In addition there may be a slight electrostrictive increase in density near the bubble surface.

The commonly accepted model for the positive charge carrier[2] is that of a He_2^+ ion which exerts an electrostrictive attraction on the surrounding liquid. Thus both pressure and density increase near the ion, in a way which can readily be calculated if the equation of state is known. There is also the possibility that, at the radius for which the pressure becomes equal to the melting pressure, there will be a liquid-solid transition resulting in a core of solid helium. A typical radius for the solid core would be about 6 Å.

Both charge carriers are therefore thought to consist of a spherical center structure plus a radial density variation $\rho(r)$ which is maintained in the surrounding fluid by electrostrictive forces. In order to correctly discuss the viscous drag force on such an object moving through a normal liquid, it is essential to realize that the increase in fluid density near the carrier will also result in a local increase in shear viscosity. If the viscosity $\eta(\rho, T)$ of the liquid is known as a function of density and temperature, then $\eta(r)$ at a given temperature can be evaluated from the calculated $\rho(r)$. Anticipating somewhat our later discussion, we show in Fig. 2 the typical behavior of $\rho(r)$ and $\eta(r)$ for the systems under consideration.

The hydrodynamic problem which therefore arises is the determination of the drag force on a spherical obstacle with radius a and velocity v_D which acts on the fluid around it so as to maintain given radial density and viscosity variations $\rho(r)$ and $\eta(r)$. We show in an Appendix to this paper that the solution of this problem can be reduced to a simple numerical procedure. The result is conveniently written in the form

$$\text{drag force} = (6\pi\eta_\infty a v_D) F \,, \tag{1}$$

where F is a dimensionless number that depends only on $\rho(r/a)\rho_\infty^{-1}$ and $\eta(r/a)\eta_\infty^{-1}$. Here ρ_∞ and η_∞ refer to the limiting values in the fluid far from the charge. If the density and viscosity are constant, then $F = 1$ for no-slip boundary conditions, and $F = \frac{2}{3}$ for perfect-slip boundary conditions. Inserted in Eq. (1), these lead of course to the standard Stokes formulas. If, however, the viscosity increases smoothly near the sphere, as is the case for our problem, F is increased above the Stokes flow value. Somewhat more surprisingly, if the density increases smoothly near the sphere, F is *decreased* below the Stokes value. Further details are found in the Appendix.

Equation (1) predicts a mobility

$$\mu = \frac{e}{6\pi\eta_\infty}\left(\frac{1}{Fa}\right) \,, \tag{2}$$

where a and F must be calculated from a specific model of the charge carrier.

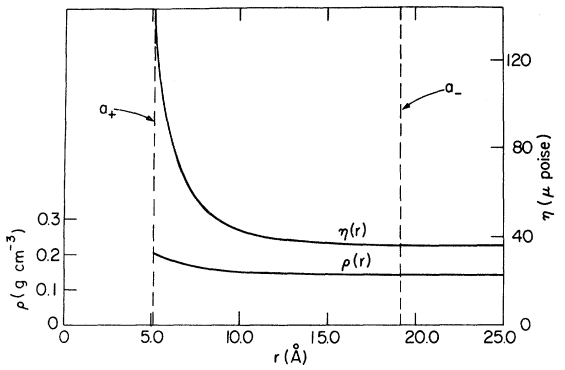

FIG. 2. Electrostrictive variation in density $\rho(r)$ and the associated variation in viscosity $\eta(r)$ near an excess charge in liquid helium at 3.0 °K.

B. Negatives below 4.2 °K

To apply Eq. (2), we need η_∞, F_-, and a_-. The viscosity of liquid He^4 at the vapor pressure has been measured by a number of authors, but only in the range $T \leq 4.2$ °K. While disagreements between various determinations have historically been large, the recent measurements of Welber[12] and Goodwin[13] agree to within 5%, which is sufficient for our purposes. It is clear from Fig. 2 that, because of the large radius of the bubble, the electrostrictive variations in ρ and η are very small. Indeed our detailed calculations show that the electrostrictive corrections to F_- are less than 1%, which is negligible compared to other errors in the analysis. Also, since the bubble approximates a free surface, the appropriate boundary conditions at $r = a_-$ should be of the perfect-slip type: $v_r = 0$, tangential stress = 0. Thus there is every reason to suppose that F_- should to a good approximation take on the perfect-slip Stokes value of $\frac{2}{3}$.

The bubble radius a_- was calculated along the vapor-pressure curve using the method of Springett, Cohen, and Jortner,[11] and including a small electrostrictive correction to the energy.[14] The total energy may be written

$$E = E_{el} + 4\pi\sigma a^2 + \tfrac{4}{3}\pi P a^3 - \tfrac{1}{2}[(\kappa - 1)/\kappa]e^2 a^{-1}, \qquad (3)$$

where E_{el} is the energy of the localized electron, σ is the surface tension of the bubble, P is the pressure, and κ is the dielectric constant of the liquid. E_{el} may be approximately calculated using the Wigner-Seitz model devised by Springett *et al.*,[11] and the resulting total energy minimized with respect to a to determine the equilibrium radius. A difficulty that arises in determining a_- is that the surface energy of the bubble is not well known. Measurements of the surface tension of liquid He^4 are available,[15] but it has been argued[16] that the tension on the bubble surface may be considerably greater. There is some evidence for such an effect: Several experiments[3,17–19] at low temperatures are best interpreted in terms of an a_- of about 15 Å, whereas the value predicted on the basis of the measured bulk surface tension is about 17.5 Å. In order to explore this further, we calculated a_- using both the measured surface tension of He^4 and 1.7 times the measured surface tension. The factor of 1.7 was chosen to yield a radius of 15 Å in the low-temperature limit, as shown in Fig. 3.

When the various terms are combined, according to Eq. (2) one obtains the curves shown in Fig. 1. Curve 1 results from using the a_- calculated from the measured surface tension; curve 2 corresponds to the enhanced values. Because of the experimental uncertainties in the viscosity, and the approximations made in calculating a_-, the comparison between theory and experiment is meaningful, at very best, to perhaps 5%. Such a comparison, however, definitely favors the idea of an enhanced surface tension, providing additional evidence for such an effect. One may also conclude that perfect-slip boundary conditions indeed seem to be correct for this system. Any other assumption lowers curves 1 and 2, leading to a worse agreement with experiment.

C. Positives below 4.2 °K

According to the model proposed by Atkins, the variation of pressure P and density ρ with radius are given by the electrostrictive equation

$$\int_{P_\infty}^{P} \frac{dP}{\rho} = \frac{\alpha_0 e^2}{2m\kappa^2 r^4}, \qquad (4)$$

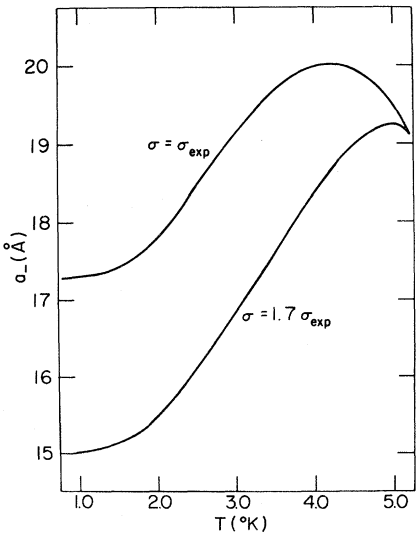

FIG. 3. Calculated radius of the electron bubble for two different assumptions about the effective surface tension at the bubble.

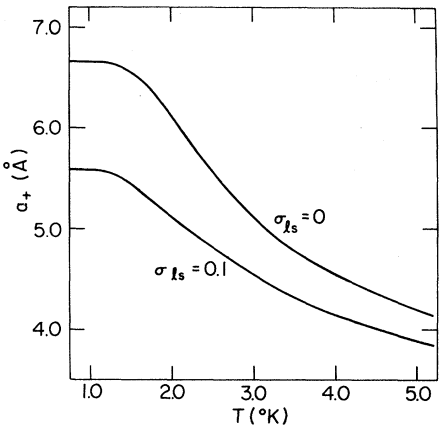

FIG. 4. Calculated radius of the positive-ion core for two different assumptions about the effective surface energy of the liquid-solid interface.

where α_0 is the atomic polarizability of He^4, m is the mass of helium atom, and the dielectric constant $\kappa = 1 + 4\pi\rho\alpha_0/m$ is a weak function of density. If the equation of state $\rho = \rho(P, T)$ is known, Eq. (4) suffices to determine $\rho(r)$ and $P(r)$. The equation of state of normal He^4 has been investigated by a number of workers,[20,21] and is sufficiently well known over the entire temperature and pressure range of interest. Our particular method of calculating $\rho(r)$ was to express the equation of state in the form

$$P = P_v(T) + \sum_{i=1}^{4} \alpha_i(T)\left(\frac{\rho}{\rho_v(T)} - 1\right)^i , \qquad (5)$$

where $P_v(T)$ is the vapor pressure, $\rho_v(T)$ is the density at the vapor pressure, and the coefficients $\alpha_i(T)$ are determined to fit the available equation-of-state data. Equation (4) can then be integrated explicitly to yield $\rho(r)$ and $P(r)$. A typical $\rho(r)$ is given in Fig. 2, which shows the results of our calculations at $T = 3.0\,^\circ$K.

In order to find $\eta(r)$ from the calculated $\rho(r)$, one needs to know $\eta(\rho, T)$ for normal He^4. This has been investigated for $T \leq 4.2\,^\circ$K by both Welber[12] and Goodwin,[13] but unfortunately their results do not agree well at high densities. We have chosen to use Goodwin's data because (a) they are more recent and are obtained by what appears to us to be a cleaner experimental method; and (b) they provide significantly better agreement with our results. At temperatures near the boiling point, it was necessary to extrapolate the measured $\eta(\rho, T)$ curves to higher densities, introducing additional uncertainties. Certain ambiguities therefore remain which can only be eliminated by more careful viscosity measurements. With these reservations, Goodwin's data can be used to obtain $\eta(r)$'s like the one shown in Fig. 2. One sees that the radial variation in the shear viscosity is typically very large, much greater than the density variation.

To complete the picture, one needs to determine a_+, the radius of the solid core which presumably surrounds the positive ion. If a possible liquid-solid surface energy σ_{ls} is taken into account, the condition determining a_+ is

$$P(a_+) = P_m(T) + 2\sigma_{ls}a_+^{-1}v_s(v_l - v_s)^{-1} , \qquad (6)$$

where $P(a_+)$ is the total pressure at a_+, $P_m(T)$ is the melting pressure, and v_s and v_l are the molar volumes of the solid and the liquid phases, respectively. All quantities in Eq. (6) can either be calculated or are well known experimentally, except for σ_{ls}. For the moment we will assume that σ_{ls} leads to only a small correction in μ_+ at the vapor pressure. This will be discussed further in Sec. III D. Curve 1 in Fig. 4 shows a_+ calculated on the assumption that $\sigma_{ls} = 0$.

Knowing $\rho(r)$, $\eta(r)$, and a_+, one can now determine the positive carrier mobility, as discussed in Sec. III A. Previous treatments of μ_+ in the normal regime have ignored the effects of $\rho(r)$, $\eta(r)$: The charge carrier is treated as a solid sphere of radius a_+, and Stokes law then yields $\mu_+ = e/6\pi\eta_\infty a_+$. Curve 3 in Fig. 1 shows that, while such a simple approach has some qualitative validity, the quantitative fit is poor. The qualitative validity arises from the way that η_∞ and a_+ enter into the exact result, Eq. (2). Because it depends only on the dimensionless functions $\rho(r/a)\rho_\infty^{-1}$, $\eta(r/a)\eta_\infty^{-1}$, F_+ turns out to be a rather weak function of temperature compared to η_∞ and a_+. Hence the temperature dependence of μ_+ is to some extent dominated by $\eta_\infty(T)$ and $a_+(T)$ in the way predicted by the simple Stokes formula.

Nevertheless, F_+ differs considerably from the Stokes value of 1. Curve 4 in Fig. 1 shows the μ_+ predicted from the electrostriction model when the hydrodynamics are treated correctly. Note that μ_+ is sharply reduced by the inclusion of $\rho(r)$ and $\eta(r)$, leading to much better quantitative agreement with experiment. The change arises almost entirely from $\eta(r)$, the effect of $\rho(r)$ alone being to increase μ_+ very slightly. Thus the physically important idea is that the electrostrictive increase in density gives rise to a greatly increased shear viscosity, and this leads to extra drag on the charge carrier.

One should note that the absolute agreement below $4.2\,^\circ$K between curve 4 and the experimental μ_+ constitutes a quite detailed verification of the electrostriction model. It indicates both the existence of a solid core of the expected size as a function of temperature, and the presence of the expected density variation in the fluid around the core. Further evidence is discussed in Sec. III D.

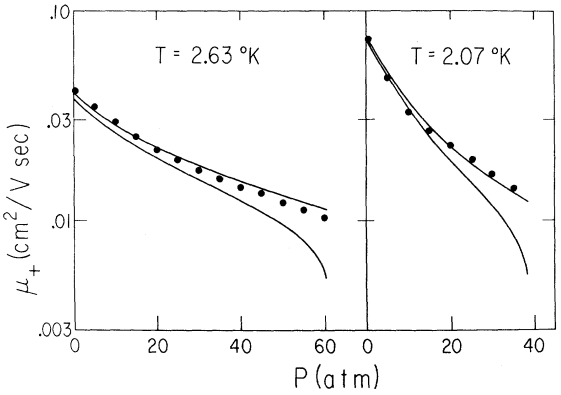

FIG. 5. Points are the data of Keshiskev *et al.* on the pressure dependence of the positive carrier mobility. The lower curves were calculated assuming $\sigma_{ls}=0$, the upper curves assuming $\sigma_{ls}=0.10$ dyne cm^{-1}.

D. Data of Keshishev *et al.*

Keshishev *et al.*[22] have measured μ_+ as a function of pressure at 2.07 and 2.63 °K. Their results, normalized to our values at the vapor pressure, are shown in Fig. 5. Although 2.07 °K is below the λ point for pressures up to about 8 atm, the normal component acts as a viscous fluid even on the scale of a few angstroms, and a hydrodynamic picture is still applicable. Treating the pressure dependence of μ_+ merely involves letting P_∞ in Eq. (4) vary, so that there is no difficulty in extending our analysis to the data shown in Fig. 5.

If $\mu_+(P_\infty)$ is calculated with the assumption $\sigma_{ls}=0$, the lower curves in Fig. 5 are obtained. The drop in μ_+ at high pressure arises because when the hydrostatic pressure in the liquid is near the melting pressure, it takes only a small additional electrostrictive pressure to cause solidification. Thus a_+ increases dramatically near the melting pressure provided $\sigma_{ls}=0$. It appears from the data that a finite surface energy prevents this from occurring,[23] and indeed it is possible to obtain a rough estimate of the σ_{ls} needed to give the observed behavior. For satisfactory agreement it was found necessary to include a value $\sigma_{ls}=(0.10 \pm 0.05)$ dyne cm^{-1} in Eq. (6), leading to the upper curves in Fig. 5.

Thus we find further confirmation for the existence of a solid core from the pressure dependence of μ_+. Curve 5 in Fig. 1 shows that including $\sigma_{ls}=0.10$ dyne cm^{-1} in the calculation of μ_+ along the vapor-pressure curve also gives a somewhat better fit, but, as assumed earlier, the correction is not very large.

E. Behavior above 4.2 °K

We now discuss briefly the interesting behavior of μ_+ and μ_- in the region above 4.2 °K. Unfortunately, no measurements of η as a function of either temperature or density seem to have been made in this region. Hence the comments which follow are, perforce, somewhat speculative. One observes two qualitative features of the data in Fig. 1. First, starting at 4.0 °K there appears to be a downward deviation of μ_+ and μ_- from the values predicted on the basis of $\eta_\infty(T)$ extrapolated from the data of Welber and of Goodwin. This is very marked for the negatives, but if curve 5 of Fig. 1 is adjusted slightly upward to fit the data at lower temperatures, it also is seen to occur for the positives. The second feature is the existence of a large drop in μ_+ beginning at $T\approx 4.7$ °K, and a much smaller but nevertheless definite kink in μ_- at $T\approx 5.1$ °K. This behavior is similar to that observed by Cantelli *et al.*[6] in He^3 near the critical point.

The carrier structures are quite different, and the only common element in determining their mobility from Eq. (2) is $\eta_\infty(T)$. One may argue therefore that features which are common to μ_+ and μ_-, such as the rapid drop just above T_λ, are likely to arise from variations in $\eta_\infty(T)$, whereas features which are quite different must be due to differences in the carrier structures. Following this line of argument, one can speculate that the downward deviation in μ_+ and μ_- above 4.2 °K arises from a $\eta_\infty(T)$ which increases in a somewhat surprising manner above the boiling point. The evidence, however, must be conceded to be weak, and direct measurements of η_∞ would be of some interest in settling the question.

More interesting and less ambiguous are the downward breaks in μ_+ and μ_-, which must certainly arise from some detail of the interaction between carrier and fluid. Since the equation of state changes rapidly near the critical point, the most obvious explanation is that the resulting changes in $\rho(r)$ and $\eta(r)$ give rise to the observed effects. Upon closer examination, however, such an explanation becomes less tenable. First, it should be pointed out that previous attempts[24,25] to explain the data of Cantelli *et al.*[6] on a hydrodynamic basis have overlooked the physical importance of the variation in shear viscosity and are therefore quite incorrect. On the other hand, one cannot evaluate μ correctly since, while $\rho(r)$ can be calculated near T_c, the important variation $\eta(r)$ cannot be determined because of the lack of viscosity data. The best one can perhaps do at this state is to try various reasonable assumptions for $\eta(\rho, T)$ in an attempt to reproduce the observed behavior. We have done many calculations of this type and our conclusion is that it cannot be done with any reasonable $\eta(\rho, T)$. The essential point is that even for T near T_c, $\rho(r)$ will be near ρ_c only at large r where electrostrictive effects are small anyway. Hence $\eta(r/a)\,\eta_\infty^{-1}$ will be modified

only slightly at large r by critical-point effects.

In sum, it appears to us very unlikely that changes in the ion structure near T_c are responsible for the sudden changes in μ_+ and μ_-: The correct treatment of the motion in the hydrodynamic approximation does not support such an explanation.

We wish to point out, however, that at some temperature close enough to T_c the hydrodynamic approximation is bound to break down because the correlation length ξ becomes too large. Near the critical point one has the approximate relation[26] $\xi = \xi_0(T_c/\Delta T)^{2/3}$, where $\xi_0 \sim 1$ Å for a typical liquid. A reasonable qualitative criterion may be that deviations from the hydrodynamic results are expected to become significant when ξ is on the order of, say, the effective radius of our probe. Because of the small size of the positive charge carrier, this occurs at the rather large value $\Delta T \sim 0.35$ °K. The corresponding ΔT for the negative carrier is about 0.06 °K. The arrows in Fig. 1 show the approximate temperatures at which one may therefore expect to see deviations caused by the critical-point fluctuations; and, in fact, the sudden drops in μ_+ and μ_- do occur there. The effect is larger for the positive charge carrier, perhaps because it is a much smaller and lighter probe than the negative carrier.

The argument given above is quite heuristic, but the agreement with experiment does suggest that the deviations near T_c may in fact arise from a breakdown of the hydrodynamic approximation due to critical-point fluctuations, rather than from changes in the ion structures as has been asserted by others. If this is indeed true, then measurements on the motion of charge carriers near T_c provide a means of studying the critical-point fluctuations in the 1–100-Å range. Further theoretical and experimental exploration of this possibility is obviously of great interest.

ACKNOWLEDGMENTS

This research has been supported in part by the Advanced Research Projects Agency. We wish to thank D. Forster for informative discussions.

APPENDIX

In this Appendix we treat the problem of calculating the drag force on a slowly moving sphere when the density and the viscosity are allowed to vary with the radial distance from the sphere. The new physical features introduced by these complications are investigated by means of simple parametric forms for $\rho(r)$ and $\eta(r)$.

A. Equation of Motion

The form taken by the Navier-Stokes equations when density and viscosity are allowed to vary is easily derived. When applied to a fluid element, Newton's law reads

$$\rho \frac{Dv_k}{Dt} = \frac{\partial}{\partial x_i}\sigma_{ik}\,, \tag{A1}$$

where ρ is the density, v_k is the kth component of the fluid velocity, D denotes the hydrodynamic derivative, and σ_{ik} is the stress tensor. The stress tensor is given by[27]

$$\sigma_{ik} = -p\delta_{ik} + \eta\left(\frac{\partial v_i}{\partial x_k} + \frac{\partial v_k}{\partial x_i} - \tfrac{2}{3}\delta_{ik}\frac{\partial v_l}{\partial x_l}\right), \tag{A2}$$

where p is the pressure and η is the shear viscosity. Combining Eqs. (A1) and (A2), one can then write the equation of motion in the vector form

$$\rho \frac{D\vec{v}}{Dt} = -\nabla p + \eta\left[\nabla^2\vec{v} + \tfrac{1}{3}\nabla(\nabla\cdot\vec{v})\right] - \tfrac{2}{3}\nabla\eta(\nabla\cdot\vec{v}) + \nabla\eta\times(\nabla\times\vec{v}) + 2(\nabla\eta\cdot\nabla)\vec{v}\,. \tag{A3}$$

The last three terms obviously arise from the nonconstancy of η. In addition to Eq. (A3), one has the equation of mass conservation

$$-\frac{\partial\rho}{\partial t} = \nabla\cdot(\rho\vec{v})\,. \tag{A4}$$

Consider a spherical obstacle of radius a centered on the origin. The fluid is assumed to be moving past the sphere such that $\vec{v} = v_\infty\hat{z}$ at infinity. The density $\rho(r)$ and the viscosity $\eta(r)$ are taken to vary in a prescribed way with the distance r from the origin, the pressure variations arising from the motion of the fluid having negligible effect on $\rho(r)$ and $\eta(r)$. We confine our discussion to the case of steady-state flow at very small Reynolds numbers. Thus, the left-hand sides of Eqs. (A3) and (A4) may be set equal to zero.

Since the divergence of $\rho\vec{v}$ is zero, one can write

$$\rho\vec{v} = \nabla\times\vec{A}\,, \tag{A5}$$

where $\vec{A}$ is a generalized stream function. It can be shown quite generally[28] that for a problem with our particular symmetry $\vec{A}$ must take the form

$$\vec{A} = -\tfrac{1}{2}rf(r)\,\hat{r}\times\hat{z}\,, \tag{A6}$$

where $f(r)$ is a function to be determined from Eq. (A3) plus the appropriate boundary conditions. The velocity is then given by

$$\rho\vec{v} = f\cos\theta\hat{r} - (f + \tfrac{1}{2}rf')\sin\theta\hat{\theta}\,, \tag{A7}$$

the primes denoting differentiation with respect to r.

The standard way to proceed is to take the curl of Eq. (A3) in order to eliminate the pressure term. One then substitutes the expression for the velocity given in Eq. (A7), obtaining a complicated fourth-order homogeneous linear differential equation for $f(r)$. We shall, however, take a somewhat different approach, designed to allow the rapid calculation of

the drag force on the sphere for given $\rho(r)$ and $\eta(r)$. Upon substituting Eq. (A7) directly into Eq. (A3), one obtains after much tedious manipulation

$$\nabla p = g_1(r)\cos\theta\hat{r} - g_2(r)\sin\theta\hat{\theta}\ , \tag{A8a}$$

where

$$g_1(r) = \left(\frac{\eta}{\rho}\right)f'' + \left(\frac{4\eta}{r\rho} - \frac{7\eta\rho'}{3\rho^2} + \frac{2\eta'}{\rho}\right)f' + \left(-\frac{2\eta\rho'}{r\rho^2} - \frac{4\eta\rho''}{3\rho^2} + \frac{8\eta\rho'^2}{3\rho^3} - \frac{4\eta'\rho'}{3\rho^2}\right)f \tag{A8b}$$

and

$$g_2(r) = \left(\frac{r\eta}{2\rho}\right)f''' + \left(\frac{3\eta}{\rho} - \frac{r\eta\rho'}{\rho^2} + \frac{r\eta'}{2\rho}\right)f'' + \left(\frac{2\eta}{r\rho} - \frac{4\eta\rho'}{\rho^2} - \frac{r\eta\rho''}{2\rho^2} + \frac{r\eta\rho'^2}{\rho^3} + \frac{\eta'}{\rho} - \frac{r\eta'\rho'}{2\rho^2}\right)f'$$
$$+ \left(-\frac{7\eta\rho'}{3r\rho^2} - \frac{\eta\rho''}{\rho^2} + \frac{2\eta\rho'^2}{\rho^3} - \frac{\eta'\rho'}{\rho^2}\right)f\ . \tag{A8c}$$

Equation (A8a) can be integrated at once to yield

$$p = rg_2(r)\cos\theta + \text{const.} \tag{A9}$$

The consistency condition

$$g_1(r) = rg_2'(r) + g_2(r) \tag{A10}$$

of course gives rise to the same fourth-order equation for $f(r)$ as that obtained by the more usual route discussed above.

Consider now the total momentum flux into a spherical surface of radius $r > a$, centered on the origin. By conservation of momentum, this must be independent of r and in fact must be equal to the total drag force F exerted on the spherical obstacle. To evaluate the total momentum flux, we integrate the stress tensor over the spherical surface:

$$\vec{F} = \hat{z}\int_s (\sigma_{rr}\cos\theta - \sigma_{\theta r}\sin\theta)r^2\sin\theta\, d\theta\, d\varphi\ , \tag{A11}$$

where

$$\sigma_{rr} = -p + \tfrac{2}{3}\eta\left(2\frac{\partial v_r}{\partial r} - \frac{2v_r}{r} - \frac{1}{r}\frac{\partial v_\theta}{\partial\theta} - \frac{v_\theta}{r\tan\theta}\right), \tag{A12a}$$

$$\sigma_{\theta r} = \eta\left(\frac{1}{r}\frac{\partial v_r}{\partial\theta} + \frac{\partial v_\theta}{\partial r} - \frac{v_\theta}{r}\right). \tag{A12b}$$

Combining Eqs. (A7)–(A12) then results in

$$f''' + \left(\frac{4}{r} - \frac{2\rho'}{\rho} + \frac{\eta'}{\eta}\right)f'' + \left(-\frac{4}{r^2} - \frac{6\rho'}{r\rho} - \frac{\rho''}{\rho} + \frac{2\rho'^2}{\rho^2} + \frac{2\eta'}{r\eta} - \frac{\eta'\rho'}{\eta\rho}\right)f' + \left(\frac{2\rho'}{r^2\rho} - \frac{2\rho''}{r\rho} + \frac{4\rho'^2}{r\rho^2} - \frac{2\eta'\rho'}{r\eta\rho}\right)f$$
$$- \frac{9\rho}{r^4\eta}F = 0\ . \tag{A13}$$

Here $\vec{v}$, η, and ρ are measured in units of their asymptotic values v_∞, η_∞, and ρ_∞; r is measured in units of the obstacle radius a; and F is measured in units of $6\pi\eta_\infty v_\infty a$.

It can readily be seen that Eq. (A13) is the first integral of Eq. (A10), with the force F playing the role of the integration constant. This constant must of course be determined from the boundary conditions. For a "no-slip" obstacle, such as a solid sphere, the fluid velocity is zero at the boundary. Then

$$f(r) = 0 \quad \text{at } r = 1\ , \tag{A14a}$$

$$f'(r) = 0 \quad \text{at } r = 1\ , \tag{A14b}$$

$$f(r) \to 1 \quad \text{as } r \to \infty\ , \tag{A14c}$$

$$rf'(r) \to 0 \quad \text{as } r \to \infty\ . \tag{A14d}$$

A "perfect-slip" obstacle such as a bubble is, on the other hand, characterized by the absence of tangential stress at the boundary; and Eq. (A14b) is changed to

$$f''(r) + \left(2 - \frac{\rho'}{\rho}\right)f'(r) = 0 \quad \text{at } r = 1\ . \tag{A14b'}$$

B. Solution

It will prove convenient to rewrite Eqs. (A13) and (A14) in terms of the variable $y = r^{-1}$. The equation of motion becomes

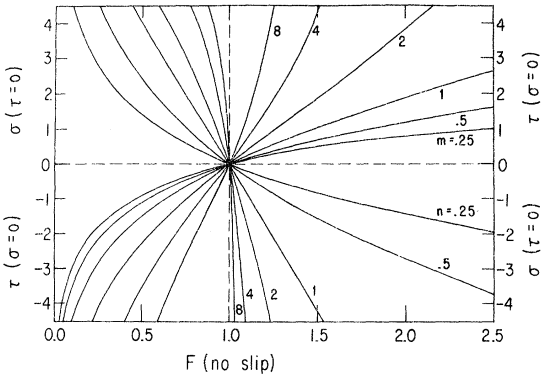

FIG. 6. Drag force for no-slip boundary conditions. Curves running from the lower left-hand corner to the upper right-hand corner are for η varying as in Eq. (A18b) and ρ constant. Those running from the upper left-hand to the lower right-hand corner are for ρ varying as in Eq. (A18a) and η constant.

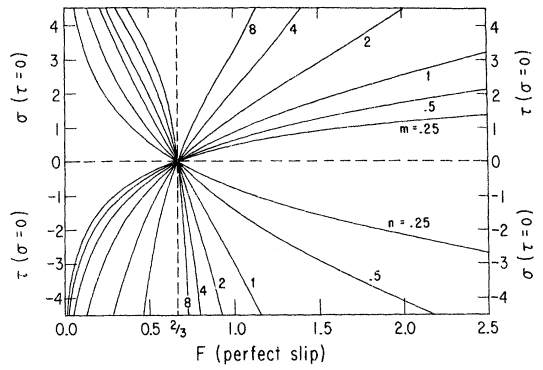

FIG. 7. Drag force for perfect-slip boundary conditions. Curves running from the lower left-hand corner to the upper right-hand corner are for η varying as in Eq. (A18b) and ρ constant. Those running from the upper left-hand to the lower right-hand corner are for ρ varying as in Eq. (A18a) and η constant.

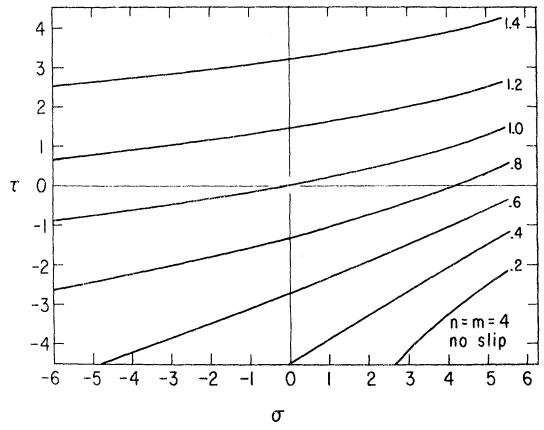

FIG. 9. Lines of constant drag force as a function of the magnitudes of the variations in ρ and η, with identical range parameters $n = m = 4$. No-slip boundary conditions.

$$y^2 f''' + \left(2y - 2y^2\frac{\rho'}{\rho} + y^2\frac{\eta'}{\eta}\right)f'' + \left(-6 + 2y^2\frac{\rho'^2}{\rho^2} - y^2\frac{\rho''}{\rho} - y^2\frac{\eta'\rho'}{\eta\rho}\right)f' + \left(6\frac{\rho'}{\rho} - 4y\frac{\rho'^2}{\rho^2} + 2y\frac{\rho''}{\rho} + 2y\frac{\eta'\rho'}{\eta\rho}\right)f + \frac{9\rho}{\eta}F = 0\,, \tag{A15}$$

while the boundary conditions go over into

$$f(y) = 0 \quad \text{at } y = 1\,, \tag{A16a}$$

$$f'(y) = 0 \quad \text{at } y = 1\,, \tag{A16b}$$

$$f(y) \to 1 \quad \text{as } y \to 0\,, \tag{A16c}$$

$$yf'(y) \to 0 \quad \text{as } y \to 0\,, \tag{A16d}$$

or, for perfect slip,

$$f''(y) - \frac{\rho'}{\rho}f'(y) = 0 \quad \text{at } y = 1\,. \tag{A16b'}$$

In Eqs. (A15) and (A16), the primes denote differentiation with respect to y.

Provided $\rho^{-1}d\rho/dr$ and $\eta^{-1}d\eta/dr$ drop off faster than r^{-1} as $r \to \infty$, Eq. (A15) has only one regular singular point in the range of interest $0 \leq y \leq 1$. Standard series-expansion methods may therefore be applied to determine $f(y)$ and F. Such an approach is not very useful, however, since even very simple functional forms for $\rho(r)$ and $\eta(r)$ lead to excessively complicated expressions, while in any case the situation of physical interest may very well involve numerically specified $\rho(r)$ and $\eta(r)$. It is virtually always more convenient to use the following trivial numerical procedure. One approximates $f(y)$ by the polynomial

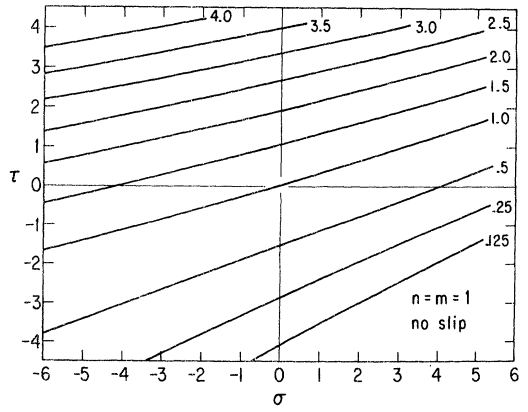

FIG. 8. Lines of constant drag force as a function of the magnitudes of the variations in ρ and η, with identical range parameters $n = m = 1$. No-slip boundary conditions.

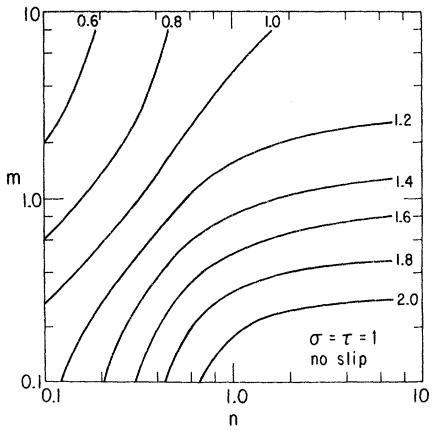

FIG. 10. Lines of constant drag force as a function of the ranges of the variations in ρ and η, with identical magnitude parameters $\sigma = \tau = 1$. No-slip boundary conditions.

$$f(y)=\sum_{i=1}^{N} a_i(y-1)^i\ , \tag{A17}$$

which satisfies Eqs. (A16a) and (A16d). Using this approximate form, Eq. (A15) is written out at the points $y=n/(N-1)$, $n=1, 2, \ldots, N-1$. In addition, one must satisfy Eq. (A16c) and either Eq. (A16b) or Eq. (A16b′). There are thus $N+1$ algebraic equations from which to determine the $N+1$ unknowns a_i and F, and F can be evaluated directly by using Cramer's rule. This method is efficient and accurate, $N=20$ usually being sufficient to determine F to seven decimal places. Of course, the great simplicity of this method arises from the fact that we chose to use the first integral, Eq. (A13), rather than Eq. (A10) as our starting point, thus allowing us to determine F without first finding f.

C. Results

We now wish to explore the physical consequences of letting ρ and η vary with radius in various ways. To do this we investigate the convenient functional forms

$$\rho=\rho_\infty e^{\sigma(a/r)^n}\ , \tag{A18a}$$

$$\eta=\eta_\infty e^{\tau(a/r)^m}\ , \tag{A18b}$$

which in our dimensionless representation become $\rho=e^{\sigma y^n}$ and $\eta=e^{\tau y^m}$. These forms were chosen because, with different values of the parameters, they can represent a large variety of smoothly increasing or decreasing behaviors for $\rho(r)$ and $\eta(r)$. Thus one might choose the asymptotic values ρ_∞, η_∞ and then pick σ and τ to obtain the desired values $\rho(a)$ and $\eta(a)$ at the sphere. Then n, m may be chosen to give the desired degree of localization of the density and viscosity disturbances near the sphere. Roughly, σ and τ determine the "magnitude" of the variation in ρ and η, respectively, while n and m determine the "range."

The effect of letting only ρ or only η vary is shown in Fig. 6 for the no-slip sphere and in Fig. 7 for the perfect-slip sphere. Several interesting qualitative conclusions can be drawn from these curves. An increase or a decrease in viscosity near the sphere leads, respectively, to a larger or smaller drag force. The magnitude of the change is a strong function of the range of r over which the increase or decrease occurs, in that disturbances which extend farther out have a much greater effect than those confined to the region near $r/a=1$. Somewhat more surprising is the conclusion that an increase in density near the sphere leads to a *decrease* in the drag force, and vice versa. The magnitude of the effect again is greater for disturbances which extend farther out. One also sees that there is no great qualitative difference in the behavior of obstacles with no-slip and perfect-slip boundary conditions.

The more general case, where both density and viscosity are allowed to vary, preserves these features. A complete discussion serves little purpose here since, for any $\rho(r)$ and $\eta(r)$ of particular physical interest, the drag force is easily computed by the numerical method outlined earlier. We therefore confine ourselves to a few cases which illustrate the types of phenomena that are encountered. First we consider how the drag force is modified in the event that the magnitudes (e^σ, e^τ) of the variations in ρ and η are allowed to vary, while the ranges are kept the same ($m=n$). Lines of equal F for no-slip boundary conditions are shown in Fig. 8 for $m=n=1$ and in Fig. 9 for $m=n=4$. The other extreme is to keep the magnitudes of the variation the same and to let the ranges vary widely. Lines of equal F for $\sigma=\tau=1$ and $\sigma=\tau=3$ are shown in Figs. 10 and 11, respectively, again for no-slip boundary conditions. Comparing Figs. 8–11 with Fig. 6 one can see that in a qualitative sense sense $\rho(r)$ and $\eta(r)$ affect F independently. That is, no matter what $\rho(r)$ is, F will increase as the magnitude and the range of the variation in $\eta(r)$ is increased. On the other hand, no matter what $\eta(r)$ is, F will decrease as the magnitude and the range of the variation of $\rho(r)$ increases. As long as the variations in $\rho(r)$ and $\eta(r)$ are not too severe, their effects are roughly additive.

Thus we see that for reasonable variations in ρ and η, such as those of Eq. (A18), Stokes's law is modified in a rather simple way. It is of course possible to investigate more pathological variations in ρ and η which might result in more startling behavior, but clearly the smoothly increasing or decreasing variations epitomized by Eq. (A18) represents the situation most likely to be found in real systems.

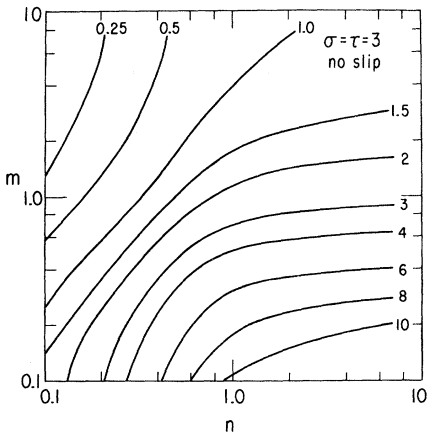

FIG. 11. Lines of constant drag force as a function of the ranges of the variations in ρ and η, with identical magnitude parameters $\sigma=\tau=3$. No-slip boundary conditions.

[1]C. G. Kuper, Phys. Rev. 122, 1007 (1961).
[2]K. R. Atkins, Phys. Rev. 116, 1339 (1959).
[3]P. E. Parks and R. J. Donnelly, Phys. Rev. Letters 16, 45 (1966).
[4]A. J. Dahm and T. M. Sanders, Jr., Phys. Rev. Letters 17, 126 (1966).
[5]K. W. Schwarz and R. W. Stark, Phys. Rev. Letters 22, 1278 (1969).
[6]R. Cantelli, I. Modena, and F. P. Ricci, Phys. Rev. 171, 236 (1968).
[7]K. W. Schwarz, Phys. Rev. Letters 24, 648 (1970).
[8]F. Reif and L. Meyer, Phys. Rev. 119, 1166 (1960).
[9]L. Meyer, H. T. Davis, S. A. Rice, and R. J. Donnelly, Phys. Rev. 126, 1927 (1962).
[10]M. Kuchnir, Ph.D. thesis (University of Illinois, Urbana, 1966) (unpublished).
[11]B. E. Springett, M. H. Cohen, and J. Jortner, Phys. Rev. 159, 183 (1967).
[12]B. Welber, Phys. Rev. 119, 1816 (1960).
[13]J. M. Goodwin, Ph.D. thesis (University of Washington, Seattle, 1968) (unpublished).
[14]T. Miyakawa and D. L. Dexter, Phys. Rev. A 1, 513 (1970).
[15]J. F. Allen and A. D. Misener, Proc. Camb. Phil. Soc. 34, 299 (1938).
[16]K. Hiroike, N. R. Kostner, S. A. Rice, and J. Jortner, J. Chem. Phys. 43, 2625 (1965).
[17]B. E. Springett, Phys. Rev. 155, 139 (1967).
[18]C. Zipfel and T. M. Sanders, *Proceedings of the Eleventh International Conference on Low Temperature Physics, St. Andrews*, 1968 (St. Andrews Printing Dept., St. Andrews, Scotland, 1968).
[19]G. Baym, R. G. Barrera, and C. J. Pethick, Phys. Rev. Letters 22, 20 (1969).
[20]J. Wilks, *Properties of Liquid and Solid Helium* (Clarendon, Oxford, 1967).
[21]P. R. Roach, Phys. Rev. 170, 213 (1968).
[22]K. O. Keshishev, Yu. Z. Kovdrya, L. P. Mezhov-Degliu, and A. I. Shal'nikov, Zh. Eksperim. i Teor. Fiz. 56, 94 (1969) [Sov. Phys. JETP 29, 53 (1969)].
[23]The necessity of including a nonzero σ_{ls} has also been pointed out by B. A. Brody, Ph. D. thesis (University of Michigan, Ann Arbor, 1970) (unpublished).
[24]E. Achter, Phys. Letters 27A, 687 (1968).
[25]B. E. Springett, Phys. Rev. 184, 229 (1969).
[26]See, for instance, H. E. Stanley, *Introduction to Phase Transitions and Critical Phenomena* (Oxford U. P., Oxford, to be published).
[27]L. D. Landau and E. M. Lifshitz, *Fluid Mechanics* (Addison-Wesley, Reading, Mass., 1959).
[28]See Ref. 27, p. 64.

PHYSICAL REVIEW A VOLUME 5, NUMBER 6 JUNE 1972

Decay of Pair Correlations

G. J. Throop and S. Fisk
Oregon Graduate Center, 19600 *N. W. Walker Road*, *Beaverton*, *Oregon* 97005
(Received 26 January 1972)

It is shown that when the second moment of the direct correlation function is negative, the usual Ornstein-Zernike analysis is inadequate. The calculation is extended and it is shown that when both the second and fourth moments are negative, the decay of correlations is oscillatory. It is then argued, following Fisher and Widom, that there will be a locus in the density-temperature plane such that at low temperatures and densities the second moment will be positive and the decay of correlations will be monotonic, while at high temperatures and densities the second and fourth moments will be negative, and the decay of correlations oscillatory.

INTRODUCTION

In a recent paper Fisher and Widom[1] discuss the asymptotic decay of the pair correlation function in one-dimensional systems. They show that when the interaction potential consists of a hard-core repulsion plus a nearest-neighbor attraction, the asymptotic decay of the correlation function can be either monotonic or oscillatory, depending on the thermodynamic state of the system. They argue that similar results will hold for three-dimensional systems, that for fluid states around the critical point the pair correlation function will be monotonic, and that for states far away from the critical point the decay will be oscillatory.

The present paper is an attempt to discuss the asymptotic form of the pair correlation function for three-dimensional systems, and to show that it is indeed possible to obtain both oscillatory and monotonic decays, depending on the thermodynamic state. Our starting point is an earlier paper of Fisher,[2] in which he discusses the Ornstein-Zernike theory in terms of the direct correlation function. The crux of Fisher's presentation is that the Fourier transform of the direct correlation function can be expanded in terms of its moments, which are defined below. Then truncation at second order and the assumption that the second moment is positive leads to the expected exponential decay. We present arguments that this second moment may in fact be negative, and that in these cases it is necessary to extend Fisher's analysis to fourth order. We are then able to show that it is possible to obtain oscillatory decay for the pair correlation function.